Evidence for coexisting prolate and near-oblate shapes at high spin in ^{125}Cs*

Ji Sun(孙吉)[1], Tetsuro Komatsubara(小松原哲郎)[2], Jia-Qi Wang(王佳琦)[1], Hao Guo(郭昊)[1], Xue-Yuan Hu(胡雪源)[1], Ying-Jun Ma(马英君)[1;1)], Yun-Zuo Liu(刘运祚)[1], Kohei Furuno(古野興平)[2]

[1] College of Physics, Jilin University, Changchun 130012, China
[2] Research Facility Center for Pure and Applied Science, University of Tsukuba, Ibaraki 305-8577, Japan

Abstract: Excited states in the odd-proton nucleus ^{125}Cs were investigated by means of in-beam γ-ray spectroscopy. The $\pi g_{7/2}$ band is observed to fork into a $\Delta I = 1$ coupled band and a $\Delta I = 2$ decoupled band at high spins. To assign the possible configurations of these two bands, experimental $B(\mathrm{M1})/B(\mathrm{E2})$ ratios and signature splittings have been evaluated for the $\Delta I = 1$ band, and calculations based on the geometrical model, cranked shell model and total Routhian surfaces model have been performed. They are suggested to be a near-oblate band built on the $(\pi g_{7/2}/d_{5/2})\otimes(\nu h_{11/2})^2$ configuration and a prolate band built on the $\pi g_{7/2}\otimes(\pi h_{11/2})^2$ configuration, respectively.

Keywords: shape coexistence, band crossing, rotational band, high spin state, ^{125}Cs

PACS: 23.20.Lv, 21.10.-k, 21.10.Re, 27.60.+j **DOI:** 10.1088/1674-1137/40/12/124001

1 Introduction

The nucleus is a unique quantum many-body system prone to deformation changes. Shape coexistence and transition have been of key interest for decades and remain at the focus of current attention. In this respect, nuclei bordering on the $Z = 50$ closed shell stand out with a rich variety of nuclear shapes accompanied by a great deal of interesting structural effects. Striking observations, e.g. band terminations with non-collective triaxiality ($\gamma = +60°$, Lund convention) [1–4] and low-spin prolate-oblate shape coexistences [5, 6], have been extensively reported. These features are intimately related to the γ-softness expected [7–10] for this nuclear region, where the potential energy surfaces are very unstable with respect to the γ-deformation. Meanwhile, individual valence nucleons occupying different orbitals may have different or even opposite shape driving effects on the core of a nucleus [8, 9]. In this region, the proton Fermi surface lies low within the $h_{11/2}$ subshell, which drives the nucleus towards a prolate shape, whereas the neutron Fermi surface lies near the middle of the $h_{11/2}$ subshell, which tries to drive the shape towards an oblate shape. Dynamic competition between prolate and oblate shapes is thereby expected, particularly at higher spins where additional unpaired $h_{11/2}$ neutrons or protons may become available.

The spherical Sn nuclei at the $Z = 50$ closed shell are well known to exhibit primarily single-particle spectra, though coexisting collective structures emerge at high spins [11]. With increasing proton number, sizable quadrupole deformation is developed and collective rotation is seen [4–6] to prevail at higher spins from $Z = 53$, allowing an easier possibility to observe the rotational breakup of paired nucleons. Because the proton Fermi surface at $Z = 53$ is still well below the $h_{11/2}$ subshell, the first bandcrossing in iodine nuclei [12] is generally from the rotational alignment of a pair of $h_{11/2}$ neutrons, for which the Fermi surface is well within the $h_{11/2}$ neutron subshell. With proton number increasing up to $Z = 56$, the proton Fermi surface has come within the proton $h_{11/2}$ subshell. Because larger Coriolis forces are expected for orbitals with lower-K values, the first bandcrossing in $Z \geqslant 56$ nuclei of this region [8, 9, 13] is believed to result generally from the rotational alignment of a pair of $h_{11/2}$ protons, which are characterized by very low-K values at prolate deformations. The $h_{11/2}$ proton and neutron crossing frequencies are thus expected to be similar in the Xe-Ba-Ce region [8, 9], and as a consequence, the ground band in a given nucleus of this region is often seen to fork into two S-bands [8, 9]. One of the two S-bands results from the $h_{11/2}$ proton alignment and the other results from the $h_{11/2}$ neutron alignment. It is often a challenge to assign the specific mechanisms for the two S-bands, particularly in the $Z = 54$ and 55 nuclei where the $h_{11/2}$ proton and neutron alignments oc-

Received 19 August 2016
∗ Supported in part by National Natural Science Foundation of China (11475072)
1) E-mail: myj@jlu.edu.cn

cur at quite similar rotational frequencies [8, 9]. In view of the opposite shape-driving forces of the $h_{11/2}$ protons and neutrons, it becomes more interesting to distinguish between the two different rotational alignments. In particular, prolate and oblate shapes may coexist at high spins due to the competing alignments and conflicting shape-driving forces of the $h_{11/2}$ protons and neutrons.

The $Z=55$ nucleus ^{125}Cs lies at the edge of the lowest $h_{11/2}$ orbital. Previous studies by us [14] and other groups [15, 16] have identified several rotational bands of this nucleus. Nevertheless, the alignment properties of its $g_{7/2}$ and $d_{5/2}$ bands have not been discussed or well understood. In particular, the $g_{7/2}$ band forks into two S-bands at high spins as the ground bands of the nearby even-even nuclei [8] do, and possible origins of the two S-bands are still elusive. Very recently, we have been given helps in the calculations of total Routhian surfaces (TRS) and the cranked shell model (CSM) based on the Woods-Saxon potentials. With the aid of these calculations, much better understandings on the shapes and quasiparticle constituents of the two S-bands in ^{125}Cs can be obtained, though a detailed level scheme of ^{125}Cs has already been reported in Ref. [14]. Particularly, as will be discussed below, the two S-bands developed from the $g_{7/2}$ band in ^{125}Cs are most likely to be coexisting prolate and oblate bands.

2 Experimental method and result

Excited states in ^{125}Cs were produced via the ^{116}Cd(^{14}N, 5n) fusion-evaporation reaction at 65 MeV bombarding energy. Details for the experimental procedure and off-line data analysis had already been described at length in our previous papers [6, 14, 17] reporting other results from the same experiment. A partial level scheme of ^{125}Cs showing the bands closely related to the present discussion is presented in Fig. 1.

In comparison with the previous studies [15, 16] on ^{125}Cs, bands 1, 3 and 5 are new bands identified from our investigation [14]. Furthermore, the hanging band 4 identified previously by Singh et al [16] has now been connected to band 2 [14]. In our construction of the present level scheme, the placement of the 842.8 keV transition shown in band 4 was complicated seriously by several contaminations from ^{126}Cs, the main product of the presently used target-projectile combination ^{116}Cd + ^{14}N. According to the level scheme proposed previously by Singh et al [16], a stronger peak at 832.6 keV than peaks at 744.1 and 865.2 keV is expected in the coincidence spectrum gating on the 842.8 keV γ-ray. However, what is seen is opposite to this expectation. When gating on the 832.6, 744.1 and 865.2 keV γ-rays to check the consistency of the level scheme proposed in Singh et al [16], our spectra are seriously contaminated by transitions with similar energies in band C reported for ^{126}Cs [18]. It seems that our two-fold γ-γ coincidence data is incapable of disentangling the observed complicated coincidence intensities associated with the 842.8 keV transition in band 4. Ignoring the inconsistency associated with coincidence intensities, the observed coincidence relations are in agreement with the level scheme proposed by Singh et al [16]. Therefore, after numerous failures in designing a satisfactory scheme for this transition, we have now accepted the scheme proposed by Singh et al. [16], considering that the nucleus ^{125}Cs was produced via the predominant 4n exit channel and the nucleus ^{126}Cs was produced only with small yields in their experiment.

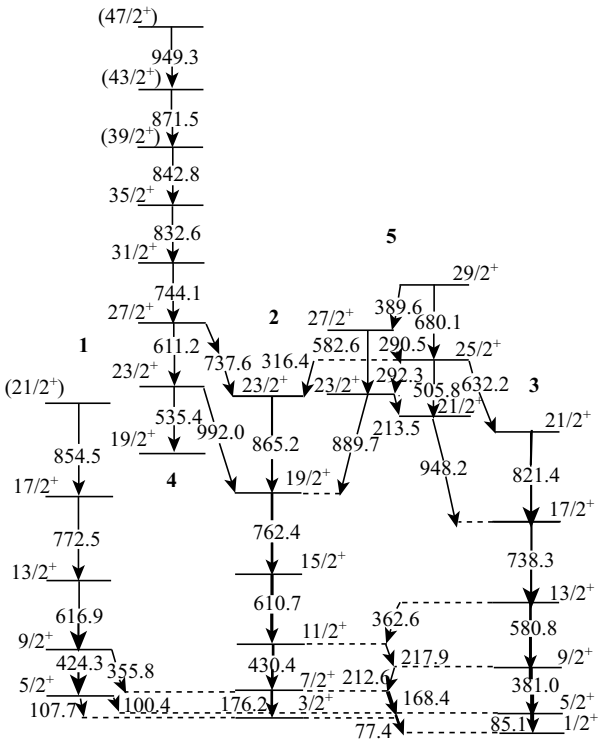

Fig. 1. Partial level scheme of ^{125}Cs as deduced from this work. Transition energies are given in keV. Transition intensities are denoted by the widths of arrows. For clarity, the levels in band 4 with $I \geqslant 31/2$ is lowered to enlarge the lower high-density part. The $19/2^+$ level in band 4 decays down to the $17/2^-$ level in the $h_{11/2}$ band; see Ref. [14].

Band 2 is known [14–16] to be based on the prolate $g_{7/2}[422]3/2^+(\alpha=-1/2)$ configuration. Considerable admixture from the nearby $d_{5/2}[420]1/2^+$ may be expected, but it does not change the intrinsic configuration on which band 2 is based at low spins. As discussed in our previous paper [14], the newly identified low-lying positive-parity bands 1 and 3 can be assigned the $g_{7/2}[422]3/2^+(\alpha=+1/2)$ and $d_{5/2}[420]1/2^+(\alpha=+1/2)$

configurations, respectively. At higher spins, the level structure reported in paper [14] has been re-arranged slightly to highlight band 5, with the relatively stronger 865.2 and 821.4 keV transitions assigned as the inband E2 transitions of bands 2 and 3, respectively. In support of the level structures relevant to bands 4 and 5, three examples of coincidence spectra are shown in Fig. 2.

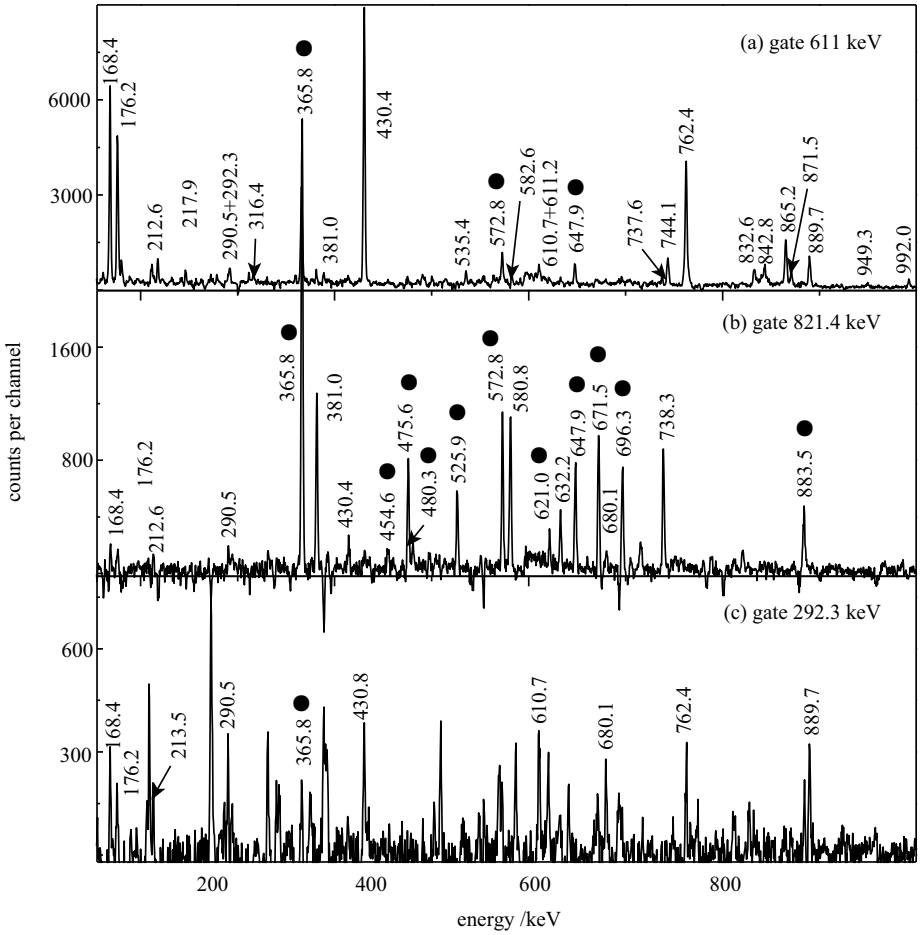

Fig. 2. Examples of coincidence spectra with gates set on (a) the 611 keV doublet γ-ray in bands 2 and 4; (b) the 821.4 keV transition in band 3; and (c) the 292.3 keV transition in band 5. Peaks marked with a solid circle are transitions in other bands of ^{125}Cs which are not shown in Fig. 1 but can be verified through the level scheme reported in Ref. [14]. Unmarked peaks in (c) are contaminations mainly from the 291.4 keV γ-ray in ^{123}I [19].

In order to search for possible clues for understanding the nature of the $\Delta I=1$ band 5, attempts have been made to extract its experimental B(M1: $I\rightarrow I-1$)/B(E2: $I\rightarrow I-2$) ratios using the well-known standard approach:

$$\frac{\mathrm{B}(\mathrm{M1}:I\rightarrow I-1)}{\mathrm{B}(\mathrm{E2}:I\rightarrow I-2)} = 0.693\frac{E_\gamma^5(I\rightarrow I-2)}{E_\gamma^3(I\rightarrow I-1)}\frac{I_\gamma(I\rightarrow I-1)}{I_\gamma(I\rightarrow I-2)}\frac{1}{(1+\delta^2)}\quad\left(\frac{\mu_\mathrm{N}}{\mathrm{e}\cdot\mathrm{b}}\right)^2, \tag{1}$$

where E_γ is in unit of MeV, I_γ is the relative intensity after normalization of detection efficiency, and δ is the M1/E2 mixing ratio. Because the mixing ratio δ is generally well below 1, the term δ^2 was neglected. Due to insufficient statistics and some contaminations, the B(M1)/B(E2) ratios could be obtained with meaningful uncertainty only at $I^\pi = 25/2^+$. When the 505.8 keV transition is regarded as the inband E2 transition of band 5, relation (1) reduces to

$$\frac{B(\mathrm{M1}:I\rightarrow I-1)}{B(\mathrm{E2}:I\rightarrow I-2)} = 0.919\frac{I_\gamma(292.3\mathrm{keV})}{I_\gamma(505.8\mathrm{keV})} = 0.707\frac{A_\gamma(292.3\mathrm{keV})}{A_\gamma(505.8\mathrm{keV})}\quad\left(\frac{\mu_\mathrm{N}}{\mathrm{e}\cdot\mathrm{b}}\right)^2, \tag{2}$$

where A_γ is the actual peak area before the normalization

of detection efficiency. With gate set on the 680.1 keV transition shown in Fig. 1, we obtained $A_\gamma(292.3\ \mathrm{keV}) = 1218 \pm 100$ and $A_\gamma\ (505.8\ \mathrm{keV}) = 543 \pm 80$, then a value of $1.6 \pm 0.6\ \mu_N^2/e^2b^2$ is obtained for the $B(M1)/B(E2)$ ratio at the $I^\pi = 25/2^+$ level in band 5. Analogously, if the 632.2 keV transition is regarded as the inband E2 transition of band 5, a ratio of $2.2 \pm 0.8\ \mu_N^2/e^2b^2$ is obtained. No transition occurs with appreciable intensity between the $23/2^+$ state in band 5 and the $21/2^+$ state in band 3, thus the 632.2 keV transition is most likely a linking transition as arranged in Fig. 1. Anyway, the $B(M1)/B(E2)$ ratio at the $I^\pi = 25/2^+$ level in band 5 is about $2\ \mu_N^2/e^2b^2$. In spite of large uncertainty, this value is consistent with the observed $\Delta I = 1$ nature of band 5. A ratio significantly smaller than this value, e.g. a value less than 0.3, would result in the un-observation of the 292.3 keV transition. Similarly, a ratio significantly larger than this value would result in the un-observation of the 505.8 keV.

3 Discussion

To gain deeper insights into the levels shown in Fig. 1, they have been transformed into a rotating coordinate according to the prescription given from CSM [20]; results are shown in Fig. 3. It is seen that: 1) band 4 crosses band 2 at $\hbar\omega = 0.39$ MeV with an alignment gain of $\Delta i_x \approx 6.0\hbar$; 2) band 5 crosses bands 2 at $\hbar\omega \approx 0.38$ MeV with an alignment gain of $6.0\hbar$; 3) band 5 crosses bands 3 at $\hbar\omega \approx 0.37$ MeV with an alignment gain of $6.5\hbar$; and 4) band 4 undergoes a second rise in alignment at $\hbar\omega \approx 0.42$ MeV with an alignment gain of $\Delta i_x \approx 4.5\hbar$. These features imply that bands 4 and 5 both are 3 quasi-particle (qp) bands at their lower spins while band 4 is a 5 qp band at its higher spins. In the even-even neighbors ^{124}Xe [3] and ^{126}Ba [13], low-lying 2 qp states built on $(\nu h_{11/2})^2$, $(\pi h_{11/2})^2$, $\nu h_{11/2}\otimes\nu g_{7/2}$ and $\pi h_{11/2}\otimes(\pi g_{7/2}/d_{5/2})$ configurations have been reported. The coupling of a valence proton in ^{125}Cs with one of the low-lying 2 qp states observed in even-even neighbors gives rise to 3 qp states near the yrast line in ^{125}Cs. As bands 4 and 5 have positive parity and appear as regular continuations of the low-lying $\pi g_{7/2}$ and $\pi d_{5/2}$ bands, candidate configurations like $\pi g_{9/2}\otimes(\nu h_{11/2})^2$, $\pi g_{9/2}\otimes(\pi h_{11/2})^2$ and $\pi h_{11/2}\otimes\nu h_{11/2}\otimes\nu g_{7/2}$ are less likely. Keeping in mind that the competition between $(\nu h_{11/2})^2$ and $(\pi h_{11/2})^2$ alignments is a characteristic feature of this region [8, 9], it seems enticing to interpret bands 4 and 5 as the forking of band 2 and the forking is caused by $(\pi h_{11/2})^2$ and $(\nu h_{11/2})^2$ alignments. On the other hand, however, bands 4 and 5 show identical initial alignments and cross band 2 at identical frequencies, which entices one to interpret them as being from the alignment of common quasiparticles.

To understand the features shown in Fig. 3, CSM calculations based on deformation parameters from self-consistent TRS [8, 21] calculations are desirable. We have therefore performed TRS calculations for ^{125}Cs, and partial results are shown in Fig. 4. The remarkable features disclosed from such TRS calculations are summarized as follows: 1) at low spins, low-lying configurations all have deformations with parameters $\beta_2 \approx 0.22$, $\beta_4 \approx 0$ and $\gamma \approx 0°$; 2) the alignments of a pair of $h_{11/2}$ protons and neutrons favor prolate shape with $\gamma \approx 0°$ (cf. Fig. 2 in Ref. [8]) and near-oblate shape with $\gamma \approx -41°$, respectively; 3) the $h_{11/2}$ neutrons align considerably earlier than the $h_{11/2}$ protons, and after $h_{11/2}$ neutron alignments, the minimum point of TRS shifts to $\gamma \approx -41°$ while the previous minimum point at $\gamma \approx 0°$ still tries to survive, giving rise to striking γ-softness as seen in Fig. 4; and 4) the alignment of $h_{11/2}$ protons occurs above 0.42 MeV, and a band termination with non-collective $\gamma = +60°$ shape as reported in ^{123}Cs [2] is expected for the lowest $(+,-1/2)$ configuration at $\hbar\omega \approx 0.48$ MeV, where much more quasiparticles have aligned their angular momenta along the symmetry axis.

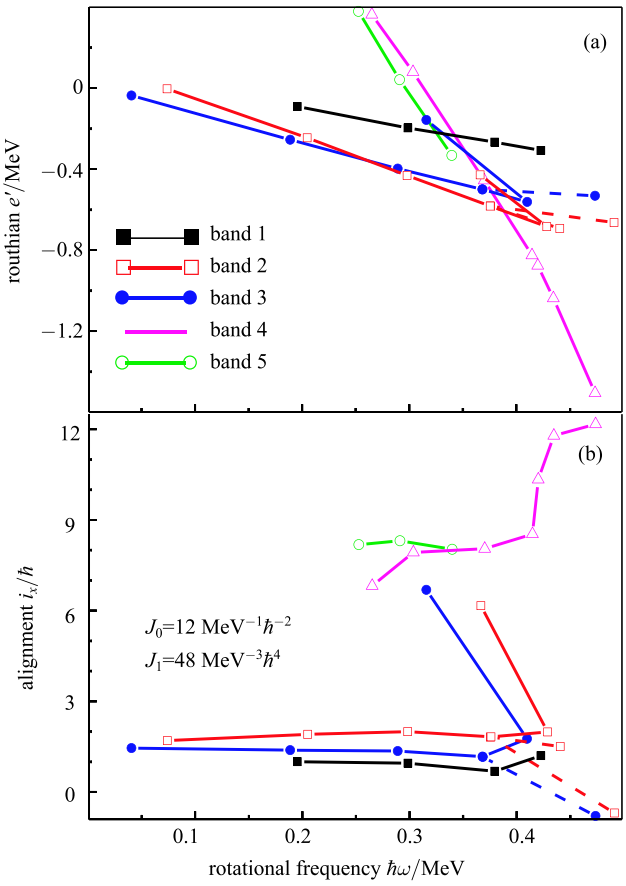

Fig. 3. (color online) Routhians and alignments for the bands shown in Fig. 1.

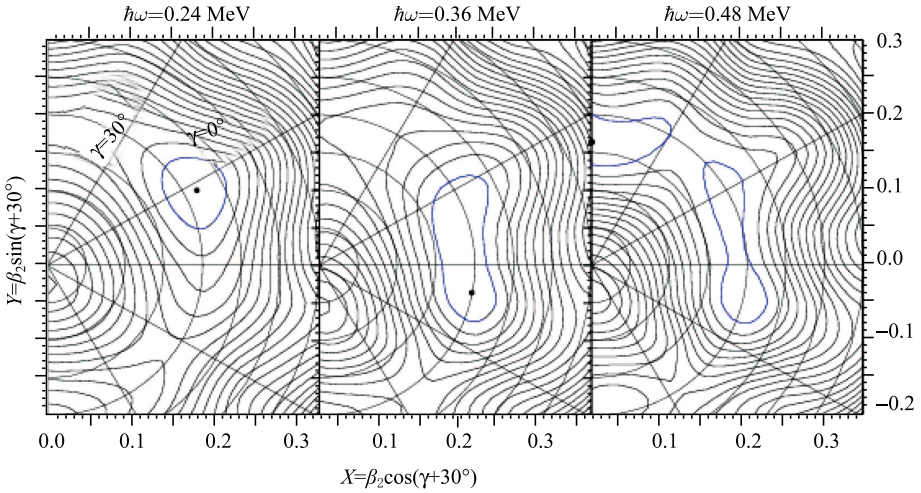

Fig. 4. Examples of TRS, calculated for the lowest $(\pi, \alpha) = (+, -1/2)$ configuration in ^{125}Cs. The energy separation between two continuous contours is 200 keV.

Utilizing the deformation parameters predicted from above TRS calculations, theoretical quasiparticle Routhians for ^{125}Cs have been calculated with the CSM based on the universal Woods-Saxon potential [21]. Representative results are shown in Fig. 5. These CSM calculations indiate that the $(\nu h_{11/2})^2$ and $(\pi h_{11/2})^2$ crossing frequencies in ^{125}Cs depends on the deformation parameters β_2 and γ to large extent. Beginning with the deformation predicted from TRS for low rotational frequencies, i.e. $\beta_2 \approx 0.22$ and $\gamma \approx 0°$, a larger β_2 or γ gives rise to a lower (higher) proton (neutron) $h_{11/2}$ crossing frequency as exhibited in Fig. 5 in Ref. [8]. Using the deformation typical for the $g_{7/2}$ and $d_{5/2}$ configurations in ^{125}Cs, CSM predicts 0.36 and 0.42 MeV for the $(\nu h_{11/2})^2$ and $(\pi h_{11/2})^2$ crossing frequencies, respectively, as seen in Figs. 5(a) and 5(b). These predictions agree reasonably well with the corresponding properties assigned [8, 3, 13] for the even-even neighbors. In the neighboring even-even nucleus ^{124}Xe (^{126}Ba), two bandcrossings at $\hbar\omega \approx 0.37$ (0.43) and 0.41 (0.39) MeV are observed and attributed to $(\nu h_{11/2})^2$ and $(\pi h_{11/2})^2$ alignments, respectively.

Because the CSM calculations as shown in Figs. 5(a) and 5(b) predict an ealier alignment for the $h_{11/2}$ neutrons than for the $h_{11/2}$ protons, the crossing of band 4 with band 2 at $\hbar\omega \approx 0.39$ MeV and the subsequent upbend at $\hbar\omega \approx 0.42$ MeV in band 4 should be attributed to the $(\nu h_{11/2})^2$ and $(\pi h_{11/2})^2$ alignments, respectively. Nevertheless, this scenario would fail to explain a significant depression in the alignment gain of the $(\pi h_{11/2})^2$ alignment. Large alignment gain is expected for the $h_{11/2}$ proton pair occupying the low-Ω $h_{11/2}[550]1/2^-$ orbital according to the CSM. As can be deduced from Fig. 5(b), the corresponding alignment gain, defined as $\Delta i_x = -\Delta e'/\Delta(\hbar\omega)$, is about 7.5 $\hbar$, which is considerably larger than the observed alignment gain of 4.5$\hbar$ associated with the second upbend in band 4. Besides, the calculation results shown in Fig. 5(c) indicates that, if the associated alignment gain is only about 4.5$\hbar$, the $(\pi h_{11/2})^2$ bandcrossing frequency would be greater than 0.6 MeV apparently inconsistent with the observations. If, instead, the successive bandcrossings observed in band 4 are attributed to a $(\pi h_{11/2})^2$ alignment followed by a $(\nu h_{11/2})^2$ alignment, a much better consistency between the observed and predicted alignment gains is seen. Under this scenario, the lower-than-expected $(\pi h_{11/2})^2$ bandcrossing frequency may be attributed to some effects which are not taken into account in the universal TRS and CSM calculations, such as the possible reduction of pair correlations of $h_{11/2}$ protons due to the presence of the $g_{7/2}$ or $d_{5/2}$ proton spectator. As to the delay of the $(\nu h_{11/2})^2$ bandcrossing in band 4, we note that very similar phenomenon has been systematically observed (see e.g. Ref. [22]) in rotational bands built on the strongly prolate-driving orbitals like $\pi h_{11/2}[550]1/2^-$ and $\pi h_{9/2}[541]1/2^-$. While a reasonable increase in quadrupole deformation can only account for a small portion of the observed delay, a more appropriate definition or treatment for the bandcrossing between two bands having very different deformations seems necessary. Anyway, though the specific reasons for the anomalous delay are still unclear, there is no dispute about the quasiparticles responsible for the bandcrossing. Actually, the observed alignment properties in band 4 agree fairly well with what are observed in the $\pi h_{11/2}$ band of ^{125}Cs [15, 16], where the bandcrossing can be umambiguously attributed to the $(\nu h_{11/2})^2$ alignment because the lowest-frequency $(\pi h_{11/2})^2$ bandcrossing is blocked. Such a close resemblance lends strong support to the above interpretation about the alignment properties of band 4.

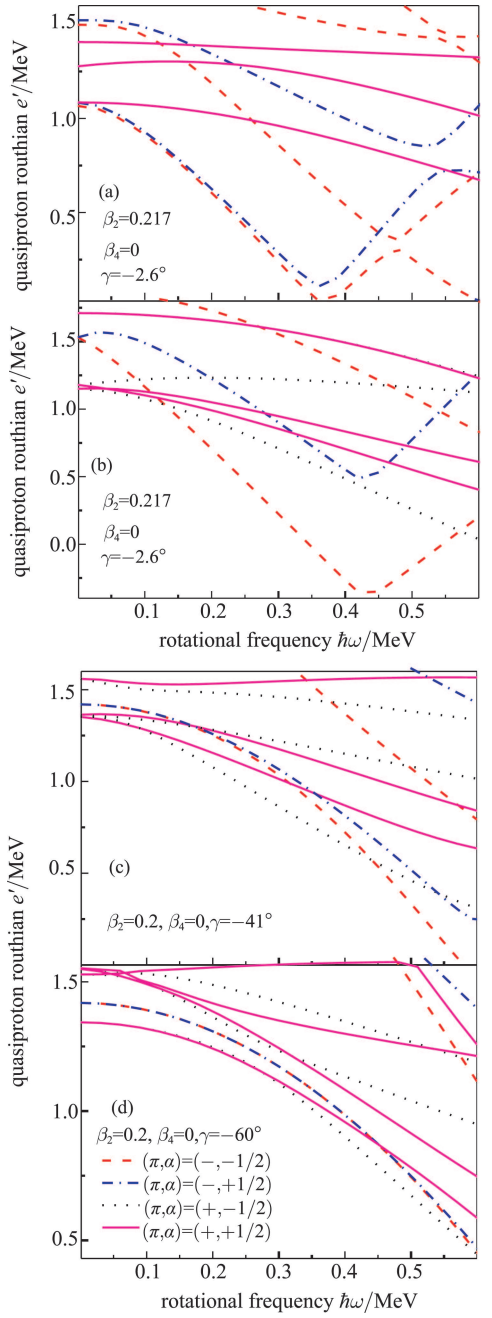

Fig. 5. (color online) Quasiparticle diagrams in ^{125}Cs, calculated with parameters given in the figure.

Experimentally, only the $\alpha = -1/2$ signature states of band 4 have been observed and the signature partner has not been observed. This suggests that the signature splitting is large and the unfavored signature of band 4 is too weakly populated to be detected in this experiment. Near the proton Fermi surface of ^{125}Cs, the $\pi g_{7/2}$ orbital is the only positive-parity orbital having the $\alpha = -1/2$ signature favored. As seen in Fig. 5(b), the corresponding trajectory keeps lying distinctly lower than the other $(\pi, \alpha) = (+, -1/2)$ trajectories over wide range of rotational frequencies. Thus, band 4 is believed to be built on the coupling of the $\pi g_{7/2}$ proton with the aligned $(\pi h_{11/2})^2$ pair and the subsequently aligned $(\nu h_{11/2})^2$ pair. According to the predictions (see Fig. 2d in Ref. [8]) of the TRS model, a prolate shape with slightly positive γ value can be expected for the $\pi g_{7/2} \otimes (\pi h_{11/2})^2$ configuration. Our extended calculations indicate that the bandcrossing frequency of 0.39 MeV and alignment gain of $6.0\hbar$ observed for the $(\pi h_{11/2})^2$ alignment in band 4 can be simultaneously reproduced by CSM at $\beta_2 = 0.23$ and $\gamma = 10°$. After the subsequent alignment of an $h_{11/2}$ neutron pair, our TRS calculation performed at $\hbar\omega = 0.48$ MeV predicts profound γ-softness and strong competition between different shapes; see Fig. 4. The regular evolution of band 4 up to the highest observed spin is a sign for a shape remaining close to prolate.

Relying solely on the comparison between observed and predicted alignment properties, it is very difficult to obtain a definite conclusion about the specific configuration for band 5. As discussed previously for band 4, the observed crossing frequency of 0.38 MeV and alignment gain of 6.0 $\hbar$ associated with band 5 can be compatible both with the $(\nu h_{11/2})^2$ and $(\pi h_{11/2})^2$ alignments. Fortunately, the $\Delta I = 1$ structure of band 5 provides additional important arguments in two respects, i.e. the signature splitting and $B(\mathrm{M1})/B(\mathrm{E2})$ ratios. By comparison with the $AI(I+1)$ law of a rotational band, a signature splitting of about 12 keV is obtained at $\hbar\omega = 0.3$ MeV for band 5, with the $\alpha = -1/2$ signature lying lower than the $\alpha = +1/2$ signature. The corresponding signature splitting between bands 1 and 2, the two signatures of the prolate $\pi g_{7/2}[422]3/2^+$ configuration [14], is about 240 keV. Band 3 is based on the prolate $\pi d_{5/2}[420]1/2^+$ configuration [14] having $\alpha = +1/2$ signature favored, and a larger signature splitting is expected for this low-Ω configuration than for the $\pi g_{7/2}[422]3/2^+$ configuration, as can be deduced from Fig. 5(b). Therefore, band 5 shows substantial decrease in signature splitting as compared both with the prolate $\pi g_{7/2}[422]3/2^+$ and $\pi d_{5/2}[420]1/2^+$ configurations, reflecting a possible drastic change in γ deformation before and after the alignment of a pair of $h_{11/2}$ protons or neutrons. Evidently, the quasiparticles responsible for such an alignment are by no means the $h_{11/2}$ protons which tend to maintain the nucleus at its prolate shape with $\gamma \approx 0°$ [8]. In contrast, the alignment of $h_{11/2}$ neutrons is expected by the TRS model to drive the nucleus towards a substantially different shape with $\gamma \approx -41°$, as seen in Fig. 4. However, the CSM calculation performed at $\gamma \approx -41°$ fails to reproduce the near to zero signature splitting observed in band 5. As seen in Fig. 5(c), the lowest $(+, -1/2)$ orbital lies lower than the lowest $(+, +1/2)$ orbital by as large as 150 keV at $\hbar\omega = 0.3$ MeV. Our extended calcula-

tions indicate that, only near the $\gamma=-60^\circ$ oblate shape, near to zero signature splitting is expected by CSM for the low-lying $\pi g_{7/2}$ orbital in ^{125}Cs; see Fig. 5(d).

To further speculate on the nature of band 5, we have performed extensive calculations of $B(\mathrm{M1})/B(\mathrm{E2})$ ratios under various assumptions according to the formula given from the geometrical model [13]:

$$\begin{aligned}&\frac{\mathrm{B(M1:}I\to I-1)}{\mathrm{B(E2:}I\to I-2)}\\&=\frac{12}{5Q_0^2\cos^2(\gamma+30^\circ)}\left[1-\frac{K^2}{(I-1/2)^2}\right]^{-2}\frac{K^2}{I^2}\\&\times\{(g_1-g_\mathrm{R})\left[\sqrt{I^2-K^2}-i_1\right]-(g_2-g_\mathrm{R})\,i_2\}^2\left(\frac{\mu_\mathrm{N}}{\mathrm{e\cdot b}}\right)^2.\end{aligned}\tag{3}$$

Equation (3) is exact only for axially symmetric nuclei, where the K quantum is conserved. For nuclei with substantial triaxial deformation, K is no longer a good quantum number. However, a substitution of K by effective K value, K_eff, may be a good approximation. The rotational gyromagnetic factor g_R is taken to be $Z/A=0.44$. The intrinsic electric quadrupole moment Q_0 in unit of e·b is computed according to the expression [23]:

$$\begin{aligned}Q_0&=ZR_0^2\frac{3}{\sqrt{5\pi}}\beta_2\left(1+\frac{2}{7}\sqrt{\frac{5}{\pi}}\beta_2\right)\\&=0.0109ZA^{\frac{2}{3}}\beta_2(1+0.36\beta_2)\end{aligned}\tag{4}$$

Using the TRS result of $\beta_2=0.2$ typical for the 3-qp bands in ^{125}Cs, a value of $Q_0=3.22$ e·b is deduced from Eq. (4). This value falls between the experimental Q_0 values [23] of the neighboring ^{124}Xe and ^{126}Ba and is therefore used in the calculation of Eq. (3). The values of g factors g_1 and g_2 are taken from Ref. [13]. The alignment parameters i_1 and i_2 are taken from Fig. 3 and adjusted slightly to meet the values expected from CSM calculations. In practice, parameters which have relatively larger effects on the final results are Q_0, K and γ. When (g_2-g_R) has the same (opposite) sign with (g_1-g_R), a reduction (enhancement) in $B(\mathrm{M1})/B(\mathrm{E2})$ is expected due to the involvement of quasiparticle(s) 2. The results of $B(\mathrm{M1})/B(\mathrm{E2})$ ratios calculated for reasonable candidate configurations are summarized in Table 1. As estimated previously using Eq. (2), a ratio lower than 0.3 will make the observation of M1 transitions of band 5 beyond the detection limit of this experiment. Therefore, the calculations shown in Table 1 exclude again the possibility of $(\pi h_{11/2})^2$ alignment which gives a $B(\mathrm{M1})/B(\mathrm{E2})$ ratio of the order of only 0.02. Meanwhile, the calculations performed at near-oblate and oblate shapes assuming $(\nu h_{11/2})^2$ alignment can provide some cases exhibiting a $B(\mathrm{M1})/B(\mathrm{E2})$ ratio consistent with the experimental value, though a specific configuration cannot be deduced definitely. Hence, the arguments from the signature splitting and from the $B(\mathrm{M1})/B(\mathrm{E2})$ ratio coherently suggest a near-oblate or oblate shape for band 5. Because the $\alpha=-1/2$ signature is observed to be lower than the $\alpha=+1/2$ signature in band 5, we suggest the $\pi g_{7/2}\otimes(\nu h_{11/2})^2$ configuration for band 5, and some admixture from $\pi d_{5/2}$ configuration into the $\pi g_{7/2}$ configuration is possible.

Table 1. $B(\mathrm{M1})/B(\mathrm{E2})$ ratios at $I^\pi=25/2^+$ calculated using Eq. (3) under different assumed configurations for band 5. $Q_0=3.22$ e·b and $g_R=0.44$ were used. For comparison, it is noted that the experimentally determined $B(\mathrm{M1})/B(\mathrm{E2})$ ratio at $I^\pi=25/2^+$ in band 5 is $1.6\pm0.6\ \mu_\mathrm{N}^2/\mathrm{e}^2\mathrm{b}^2$. Configurations yielding results consistent with the experiment are marked with an asterisk *.

assumed configuration	$\gamma/(^\circ)$	g_1	g_2	$i_1/\hbar$	$i_2/\hbar$	K_eff	$B(\mathrm{M1})/B(\mathrm{E2})$ $(\mu_\mathrm{N}^2/\mathrm{e}^2\mathrm{b}^2)$
$\pi g_{7/2}[422]3/2^+\otimes(\pi h_{11/2})^2$	10	0.72	1.17	1.5	7.8	3/2	0.04
$\pi d_{5/2}[420]1/2^+\otimes(\pi h_{11/2})^2$	10	1.38	1.17	0.7	7.8	1/2	0.02
$\pi g_{7/2}[422]3/2^+\otimes(\pi h_{11/2})^2$	0	0.72	1.17	1.2	7.1	3/2	0.02
$\pi d_{5/2}[420]1/2^+\otimes(\nu h_{11/2})^2$	0	1.38	−0.21	0.7	5.6	1/2	0.11
$\pi g_{7/2}[422]3/2^+\otimes(\nu h_{11/2})^2$	0	0.72	−0.21	1.2	5.6	3/2	0.21
* $\pi g_{7/2}\otimes(\nu h_{11/2})^2$	−41	0.72	−0.21	1.2	7.5	3.5	1.40
$\pi g_{7/2}\otimes(\nu h_{11/2})^2$	−41	0.72	−0.21	1.2	7.5	2.5	0.67
$\pi g_{7/2}\otimes(\nu h_{11/2})^2$	−41	0.72	−0.21	1.2	7.5	1.5	0.23
* $\pi d_{5/2}\otimes(\nu h_{11/2})^2$	−41	1.38	−0.21	0.6	7.5	2.5	2.63
* $\pi d_{5/2}\otimes(\nu h_{11/2})^2$	−41	1.38	−0.21	0.6	7.5	1.5	0.91
$\pi d_{5/2}\otimes(\nu h_{11/2})^2$	−41	1.38	−0.21	0.6	7.5	0.5	0.10
* $\pi g_{7/2}[404]7/2^+\otimes(\nu h_{11/2})^2$	−60	0.72	−0.21	0.6	6.8	7/2	1.67
$\pi d_{5/2}[402]5/2^+\otimes(\nu h_{11/2})^2$	−60	1.38	−0.21	0.7	6.8	5/2	3.15

It seems there is an alternative scenario for interpreting band 5 as described in the following. The so-called $\alpha=-1/2$ and $+1/2$ signatures of band 5 are not forming a $\Delta I=1$ band built on a common configuration; they can be understood as two individual continuations of bands 2 and 3, respectively. However, because the $(\pi h_{11/2})^2$ and $(\nu h_{11/2})^2$ alignments have both been assigned in the near-prolate band 4, one has to assign the $\alpha=-1/2$ signature of band 5 as a near-oblate structure built either on the $(\pi h_{11/2})^2$ or $(\nu h_{11/2})^2$ alignment. Thus, this scenario has no essential difference from the previous one. Besides, it is more reasonable to interpret the two signature sequences in band 5 as forming a $\Delta I=1$ band. It is also noted that band 5 is unlikely a magnetic rotational band because the nucleus ^{125}Cs is well deformed.

A $\Delta I=1$ band assigned to the $\pi h_{11/2}\otimes\nu h_{11/2}\otimes\nu g_{7/2}$ configuration is intensely populated in many odd-Z nuclei in this region, but its counterpart band in ^{125}Cs [14] is a band which is not shown in Fig. 1. Structures similar to bands 4 and 5 have also been observed in a few other odd-A Cs isotopes. In ^{123}Cs [2, 24], a $\Delta I=2$ decoupled band analogous to band 4 is assigned to the prolate $\pi g_{7/2}\otimes(\pi h_{11/2})^2$ configuration at low spins and to the $\pi g_{7/2}\otimes(\pi h_{11/2})^2\otimes(\nu h_{11/2})^2$ configuration at higher spins. In ^{127}Cs [25], a dipole band with some transitions nearly identical to the dipole transitions in band 5 is assigned to the oblate $\pi d_{5/2}\otimes(\nu h_{11/2})^2$ configuration. These interpretations are compatible with the present interpretations for bands 4 and 5. Moreover, the observation of bands 4 and 5 in ^{125}Cs represents a case where both the prolate band like that in ^{123}Cs and the oblate band like that in ^{127}Cs are observed at high spin simultaneously. Similar to the case of ^{125}Cs, evidence for coexisting prolate and oblate structures built on the $\pi h_{11/2}\otimes(\nu h_{11/2})^2$ configuration has been reported in ^{129}Cs [26,27].

4 Summary

In summary, excited states in ^{125}Cs were populated via the ^{116}Cd(^{14}N, 5n) reaction. It is demonstrated that the $g_{7/2}$ band forks into two structures with increasing spin. One of the bands shows $\Delta I=1$ coupled structure and the another shows $\Delta I=2$ decoupled structure. Experimental Routhians and alignments, signature splittings and $B(\mathrm{M1})/B(\mathrm{E2})$ ratios are extracted and then compared with the expectations from TRS, CSM and geometrical models. It is argued that the $\Delta I=1$ band is built on the $(\pi g_{7/2}/d_{5/2})\otimes(\nu h_{11/2})^2$ configuration with near-oblate or even oblate shape whereas the $\Delta I=2$ band results from the $(\pi h_{11/2})^2$ alignment at a $\gamma\approx 0^\circ$ prolate shape followed by a subsequent $(\nu h_{11/2})^2$ alignment.

We wish to thank the GAMMA group at the China Institute of Atomic Energy for their help in the TRS calculations.

References

1 C. M. Parry et al, Phys. Rev. C, **61**: 021303 (2000)
2 A. K. Singh et al, Phys. Rev. C, **70**: 034315 (2004)
3 A. Al-Khatib et al, Eur. Phys. J. A, **36**: 21 (2008)
4 Gong-Ye Liu et al, Chin. Phys. Lett. **29**: 092301 (2012)
5 Y. Liang, D. B. Fossan, J. R. Hughes, D. R. LaFosse, T. Lauritsen, R. Ma, E. S. Paul, P. Vaska, M. P. Waring, N. Xu, Phys. Rev. C, **45**: 1041 (1992)
6 S-Y Wang et al, J. Phys. G, **32**: 283 (2006)
7 I. Ragnarsson, A. Sobiczewski, R. K. Sheline, S. E. Larsson, B. Nerlo-Pomorska, Nucl. Phys. A, **233**: 329 (1974)
8 R. Wyss et al, Nucl. Phys. A, **505**: 337 (1989)
9 A. Granderath, P. E. Mantica, R. Bengtsson, R. Wyss, P. von Brentano, A. Gelberg, E Seiffert, Nucl. Phys. A, **597**: 427 (1996)
10 Q. Yang, H. -L. Wang, Q. -Z. Chai, M. -L. Liu, Chin. Phys. C, **39**: 094102 (2015)
11 S. Y. Wang et al, Phys. Rev. C, **81**: 017301 (2010)
12 S. Y. Wang et al, Chin. Phys. Lett., **21**: 1024 (2004)
13 D. Ward et al, Nucl. Phys. A, **529**: 315 (1991)
14 Ji Sun et al, Phys. Rev. C, **93**: 064301 (2016)
15 J. R. Hughes, D. B. Fossan, D. R. LaFosse, Y. Liang, P. Vaska, and M. P. Waring, Phys. Rev. C, **44**: 2390 (1991)
16 K. Singh et al, Eur. Phys. J. A, **27**: 321 (2006)
17 T. Komatsubara et al, Nucl. Phys. A, **557**: 419c (1993)
18 S. -Y. Wang, Y. -Z. Liu, Y. -J. Ma, T. Komatsubra and Y. -H. Zhang, Phys. Rev. C, **75**: 037302 (2007)
19 R. Goswami, B. Sethi and P. Banerjee, Phys. Rev. C, **47**: 1013 (1993)
20 R. Bengtsson and S. Frauendorf, Nucl. Phys. A, **327**: 139 (1979)
21 W. Nazarewicz, J. Dudek, R. Bengtsson, T. Bengtsson and I. Ragnarsson, Nucl. Phys. A, **435**: 397 (1985)
22 Ying-Jun Ma et al, J. Phys. G, **26**: 43 (2000)
23 S. Raman, C. W. Nestor Jr., and P. Tikkanen, Atomic Data Nucl. Data Tab., **78**: 1 (2001)
24 Kuljeet Singh et al, Eur. Phys. J. A, **25**: 345 (2005)
25 Y. Liang, R. Ma, E. S. Paul, N. Xu, D. B. Fossan and R. Wyss, Phys. Rev. C, **42**: 890 (1990)
26 S. Sihotra et al, Phys. Rev. C, **79**: 044317 (2009)
27 Yan-Xin Zhao et al, Chin. Phys. Lett., **26**: 092301 (2009)